JOURNAL OF GEOPHYSICAL RESEARCH, VOL. 113, A08302, doi:10.1029/2008JA013089, 2008

Meridional winds derived from COSMIC radio occultation measurements

Xiaoli Luan[1] and Stanley C. Solomon[1]

Received 10 February 2008; revised 18 March 2008; accepted 31 March 2008; published 5 August 2008.

[1] Meridional winds at the magnetic meridian in the upper thermosphere are derived from the peak height and density of the ionospheric F_2 layer as retrieved by the Constellation Observing System for Meteorology, Ionosphere, and Climate (COSMIC) satellites for 4 months from November 2006 to February 2007. These winds (referred to as COSMIC winds) are first validated by comparison at multiple locations with winds obtained from ground-based incoherent scatter radar (ISR) and Fabry-Perot interferometer (FPI) measurements. Then longitudinal variations of these winds are investigated and compared with simulations by the National Center for Atmospheric Research Thermosphere-Ionosphere-Electrodynamics General Circulation Model (NCAR TIE-GCM). The results show generally good agreement between COSMIC winds, ground-based measurements, and the simulations. Significant longitudinal variations are presented in the COSMIC winds. At 40°N (local winter), around midnight the COSMIC winds exhibit stronger and longer-duration equatorward velocities within 110°W–20°W (large negative magnetic declination sector) than those in other longitudes; during late morning hours the poleward winds show similar longitudinal variations. At 40°S (local summer), during the daytime the poleward winds are stronger within 120°E–110°W (large positive magnetic declination sector) than in 60°W–90°E (large negative magnetic declination sector), while during the nighttime the maximum equatorward winds shifts about 2 h later in 60°W–90°E than in 120°E–110°W. Analysis of the TIE-GCM simulations suggests that the longitudinal variation of meridional winds is mainly induced by magnetic declination due to the contribution of geographic zonal wind.

Citation: Luan, X., and S. C. Solomon (2008), Meridional winds derived from COSMIC radio occultation measurements, *J. Geophys. Res.*, *113*, A08302, doi:10.1029/2008JA013089.

1. Introduction

[2] The neutral meridional winds along the magnetic meridian or equivalent winds can be derived from F2-layer peak height (hmF_2) and peak density (NmF_2) due to the proportional relationship between the winds and the variation of the F2-layer peak height [*Rishbeth*, 1967; *Rishbeth et al.*, 1978; *Miller et al.*, 1986, 1997; *Richards*, 1991; *Buonsanto et al.*, 1989, 1997; *Liu et al.*, 2003a]. The hmF_2 and NmF_2 have been routinely observed by global ground ionosondes for decades. Therefore many studies have taken efforts to investigate the characteristics of the magnetic meridional winds or equivalent winds derived from the hmF_2 and NmF_2. The diurnal, seasonal, solar cycle and also latitudinal variations of these winds have been widely studied through the measurements from ionosode stations in the world under magnetically undisturbed condition [*Buonsanto*, 1990, 1991; *Igi et al.*, 1995, 1999; *Miller et al.*, 1997; *Foppiano et al.*, 2003; *Liu et al.*, 2003b, 2004; *Luan et al.*, 2004]. On the other hand, winds in the upper thermosphere have been observed by Fabry-Perot interferometer (FPI) during the night and derived from Incoherent Scatter Radar (ISR) observation, but only at limited stations. The climatology of winds have also been studied in these FPI and ISR stations [*Duboin and Lafeuille*, 1992; *Hagan*, 1993; *Biondi et al.*, 1999; *Buonsanto and Witasse*, 1999; *Kawamura et al.*, 2000; *Emmert et al.*, 2003, 2006]. However, the detailed behaviors of the neutral winds are still not fully understood. Conflicts in characteristics of the winds, such as the amplitude and solar cycle variation, are not only found among those derived from different techniques, but also among those at different locations [*Hedin et al.*, 1994; *Liu et al.*, 2004].

[3] A striking characteristic of the neutral winds is their geographic dependence. Strong latitudinal dependence of the meridional winds or equivalent winds has been reported over Millstone Hill [*Emmert et al.*, 2003], in the east Asian-Australian sector (120°–150°E) [*Luan et al.*, 2004], in the Antarctic Peninsula longitude sector [*Foppiano et al.*, 2003], and also at multiple stations in the world [*Miller et al.*, 1997; *Liu et al.*, 2004]. Longitudinal variations of neutral winds have also been found, but they were seldom investigated in detail before due to sparse observations. *Hedin et al.* [1994] suggested that great longitudinal vari-

[1]High Altitude Observatory, National Center for Atmospheric Research, Boulder, Colorado, USA.

0148-0227/08/2008JA013089$09.00

ation of the meridional winds existed, although those winds were observed or derived from different source at different locations (e.g., from ISR and FPI for Millstone Hill, from ISR for Saint Santin, and from ionosonde for Boulder, and also from both empirical and theoretic models for all the locations). Large differences also occur between the HWM90/93 model [*Hedin et al.*, 1991, 1996] and winds derived from ionosonde observations in East Asian-Australian sector [e.g., *Miller et al.*, 1997; *Liu et al.*, 2003b; *Luan et al.*, 2004], which are attributed in part to the dominant database at the American sector for the model construction. Similarly, the MU radar winds in Shigaraki, Japan are reported to be different from the HWM model winds in seasonal and solar activity variations [*Kawamura et al.*, 2000]. In addition, observations of several satellites have revealed significant and large-scale longitudinal variation of ionosphere structure, suggesting corresponding longitudinal variations of the associated meridional winds [*Forbes et al.*, 1997; *de Paula et al.*, 2002; *Deminova*, 2002; *Kil et al.*, 2006]. The few works that took efforts to examine the detailed longitudinal variations in the upper thermosphere include the study of zonal winds in the equatorial regions observed by the DE-2 satellite [*Wu et al.*, 1994] and derived from CHAMP satellite accelerometer measurements [*Häusler et al.*, 2007].

[4] Due to close coupling between neutral winds and upper ionospheric structure [e.g., *de Paula et al.*, 2002; *Kil et al.*, 2006], it is of considerable interest to examine the longitudinal dependence of neutral winds. Examination of the longitudinal variation of the upper thermosphere winds is hampered by the sparseness of the available data. Even ionosonde observations are lacking in oceanic areas, especially in the Southern Hemisphere. At present the Constellation Observing System for Meteorology, Ionosphere, and Climate (COSMIC) observations from six satellites can provide a global coverage of the retrieved F2-layer peak height and peak density. Therefore the average meridional winds can be derived globally in the same way they are derived from ionosonde observations under magnetically quiet conditions. The important purpose for the present study is to contribute to the limited information on the longitudinal variations of the upper thermosphere winds and their mechanisms at midlatitudes using the COSMIC observations.

[5] First, to validate this new database, the derived winds are compared with various observations (ISR, FPI if available) and with simulations of the National Center for Atmospheric Research Thermosphere-Ionosphere-Electrodynamics General Circulation Model (NCAR TIE-GCM). Comparisons at the stations of Millstone Hill, Saint Santin, Arecibo, and Shigaraki are presented. Then the detailed longitudinal variations of the magnetic meridional winds at 40°N and 40°S are discussed using the COSMIC observations during the period of northern winter (November 2006 to February 2007). Finally, the longitudinal pattern of COSMIC winds is compared with TIE-GCM simulation and its mechanisms are investigated.

2. Data Set and Method of Analysis

2.1. NmF_2 and hmF2 From COSMIC Radio Occultation Measurements

[6] The Constellation Observing System for Meteorology, Ionosphere, and Climate (COSMIC), consisting of six identical microsatellites, was launched on 15 April 2006 [*Schreiner et al.*, 2007]. The instruments employed in this paper are the Global Positioning System (GPS) radio occultation (RO) receivers. The phase delay of the RO signal propagating between GPS and COSMIC satellites, which depends on the atmosphere and ionosphere refractivity, are measured, and hence the electron density profile can be retrieved based on the proportional relationship between the refractivity and ionospheric electron column density [see *Lei et al.*, 2007a]. The NmF_2 and hmF_2 are then derived from electron density profiles. According to the work of *Lei et al.* [2007a], good agreements are achieved between COSMIC retrieved NmF_2 values and those measured by globally distributed ionosondes with the correlation coefficient as high as 0.85; and the global map of hmF_2 retrieved from COSMIC is in reasonably good agreement with empirical model and NCAR TIE-GCM. Both the hmF_2 from COSMIC and TIE-GCM will be also presented in this work. The data used in this analysis are during the 4 months from November 2006 to February 2007. During this period the observation had reasonable global coverage, with valid F_2 layer peak density and height data varying from about 1400 points to 2600 points per day.

[7] To have a good local time coverage, the NmF_2 and hmF_2 data are binned within ±2.5° intervals in latitude and ±15° in longitude. Then all the binned data in each analyzed sample location are sorted by their local time to get the averaged NmF_2 and hmF_2 every 15 min using 1 h moving window. Using this method, the NmF_2 and hmF_2 data are binned, with the latitude and longitude intervals centered at the four particular locations of Millstone Hill (42.6°N, 71.5°W), Saint Santin (44.6°N, 2.2°E), Arecibo (18.3°N, 66.7°W), and the middle and upper atmosphere (MU) radar in Shigaraki (35°N, 136°E). At these stations the ISR and/or FPI winds are available. Similarly, the average NmF_2 and hmF_2 data are obtained at central latitudes of 40°N and 40°S with analyzed grids divided by 10° in longitude, hence we adopted total 36 sample analyzed locations at each latitude. Data when the daily geomagnetic Ap index is higher than 20 are excluded. At least 10 occultation profiles are required for each binned local time. Figure 1 presents an example of the F_2 layer peak height and peak electron density data with standard deviations over Millstone Hill. It shows that the observational sampling is adequate at each local time, while large day-to-day variability of hmF_2 can be seen at night. Similar results can be obtained at Arecibo, Shigaraki, Saint Santin, and all the sample locations at 40°N and 40°S. The data sampling is relatively sparse (<15) during 0230–0400 LT over Millstone Hill and during 1200–1500 LT over the MU radar. For each selected station and each sample location at 40°N and 40°S, the number of observational sampling points is within the range of 500–650.

2.2. Determination of Meridional/Equivalent Wind

[8] The servo model by *Rishbeth* [1967] and *Rishbeth et al.* [1978] gave a detailed description of the relationship between the meridional wind and the F_2 layer peak height change from a balance height. The balance height is assumed to be the peak height of F_2 layer determined by loss and diffusion in the absence of any applied drift induced by neutral winds and electric field. The applied

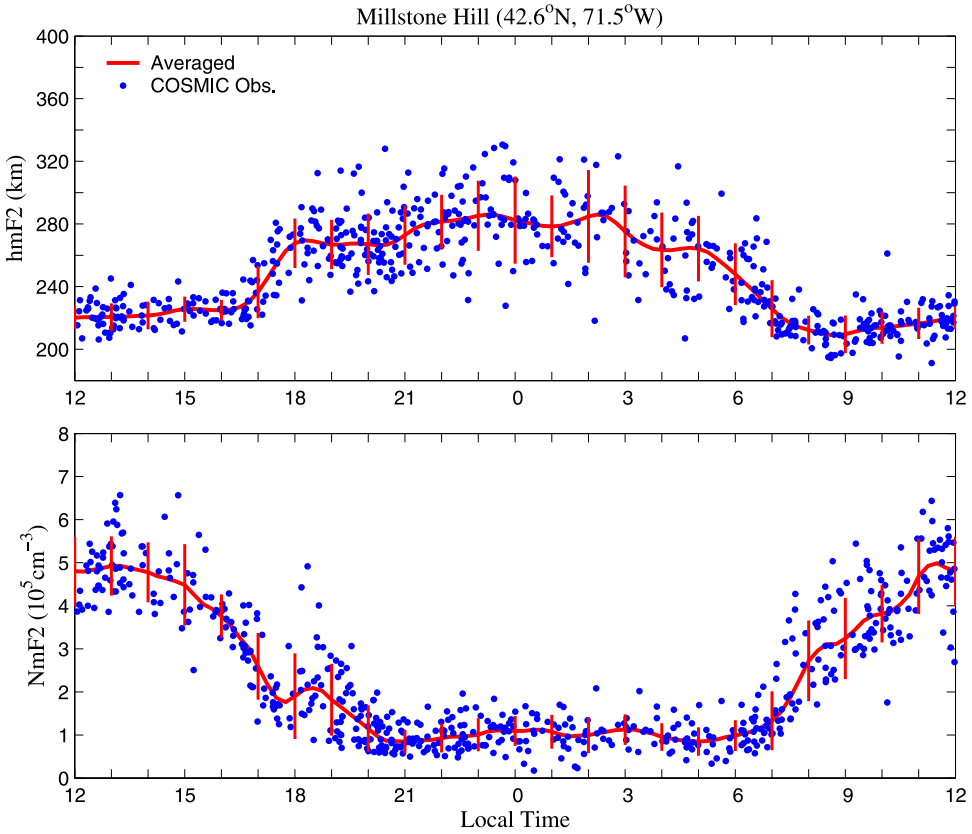

Figure 1. The averaged F_2 layer peak height hmF_2 (top) and peak density NmF_2 (bottom) with their standard deviations over Millstone Hill (42.6°N, 71.5°W). The original observations from COSMIC are also presented.

vertical drifts can be expressed in the following [see *Buonsanto et al.*, 1989, 1997]:

$$W = H\frac{dz}{dt} + D\frac{sin^2 I}{2H}[e^z - e^{-kz}] \quad (1)$$

Where W is the vertical drift; H is the scale height of the atomic oxygen and I is the magnetic dip angle; $z = (hmF_2 - h_0)/H$ is the reduced height, where h_0 is the balance height; $D = D_{in}(1 + T_e/T_i)$ is the diffusion coefficient, in which D_{in} is the ion-neutral diffusion coefficient.

[9] For the servo model the steady state conditions are assumed, hence only winds under magnetically undisturbed conditions can be obtained [*Rishbeth et al.*, 1978; *Richards*, 1991]. In these calculations, ion and electron temperatures are obtained from the empirical IRI-2001 model [*Bilitza*, 2001], and the neutral density and temperature from MSISE00 model [*Picone et al.*, 2002]. The empirical servo constant is adjusted by a factor of 0.75 from the value introduced by *Rishbeth et al.* [1978], as recommended by *Buonsanto et al.* [1997] based on comparisons over Millstone Hill. Also, a Chapman-β layer is assumed for the electron density profile of the topside [*Luan et al.*, 2004]. Among all the input parameters to calculate the meridional winds, the hmF_2 and ion-neutral collision frequency are the most important ones.

[10] The magnetic meridional wind (V_M, equatorward positive) can then be expressed as in equation (2), in which the effect of north-perpendicular $\mathbf{E} \times \mathbf{B}$ drift ($V_{\perp N}$) can be ignored at middle latitudes under conditions without large geomagnetic disturbances [*Miller et al.*, 1997]:

$$V_M = \frac{W - V_{\perp N}\cos I}{\cos I \sin I} \approx \frac{W}{\cos I \sin I} \quad (2)$$

where W is the vertical drift/equivalent wind in equation (1) and I is the magnetic dip angle.

2.3. Winds From ISR and FPI Techniques

[11] Fabry-Perot interferometers (FPI) measure the Doppler shift of the 630 nm atomic oxygen emission line at an average altitude of 250 km, from which vector horizontal winds can be obtained. FPI observations over Millstone Hill (during 1989–2001) and Arecibo (during 1980–1999) were obtained from the CEDAR Database (http://cedarweb.hao.ucar.edu). At these two stations, FPI winds are averaged under low F10.7 (<100) and low daily Ap (<20) conditions from all the available observations in winter months, and then used in the following comparisons. The FPI observations include south-looking and north-looking observations at Millstone Hill. The south-looking observation represents an averaged latitude of ~40°N, while the north-looking one is at ~45°N [*Emmert et al.*, 2003]. A detailed description of FPI wind measurements at Arecibo has been given by *Biondi et al.* [1999].

[12] The ISR wind measurement technique calculates the magnetic meridional wind from the field-aligned component

of the plasma drift velocity ($V_{\parallel}$) after subtracting the ion diffusion velocity. The ISR winds compiled here are from the published results by *Duboin and Lafeuille* [1992] over Saint Santin, by *Buonsanto and Witasse* [1999] over Millstone Hill, and by *Kawamura et al.* [2000] over Shigaraki (MU radar). For these ISR winds, the O^+–O collision frequency given by *Banks* [1966] (or similar formula) was multiplied by a Burnside factor [*Burnside et al.*, 1987] of 1.3, except that at Saint Santin a factor of about 1.7 is used [*Duboin and Lafeuille*, 1992]. The Burnside factor of 1.3 is also used in the servo wind derivation and in the TIE-GCM simulations.

2.4. TIE-GCM Simulations

[13] Simulations from the NCAR TIE-GCM [*Roble et al.*, 1988; *Richmond et al.*, 1992] are performed, for winter solstice, day number 355 of 2006 under low solar activity ($F_{10.7}$ = 80) and magnetically quiet conditions (hemisphere power = 12 GW and cross-polar-cap potential = 46.5 kV), similar to the solar and geomagnetic conditions of the COSMIC observations. Neutral winds are then obtained at an altitude near 300 km. Several updates and improvements to the TIE-GCM have been made since the version used in previous comparisons by *Hedin et al.* [1994], and it has been shown to reproduce winds well over Shigariki, Japan [*Lei et al.*, 2007b].

[14] For both the FPI and TIE-GCM winds, the magnetic meridional winds (V_M, referred to as meridional winds in the following) are obtained from meridional winds (V_G, equatorward positive, referred to as north-south winds in the following) and zonal winds (U_G, eastward positive) in geographic coordinates, using the magnetic declination angle (D), as expressed by equation (3):

$$V_M = V_G \cos(D) \mp U_G \sin(D), \tag{3}$$

where the signs "−" and "+" correspond to winds in the Northern and Southern Hemisphere, respectively.

3. Results

3.1. Comparison With ISR/FPI and TIE-GCM Winds

[15] Figure 2 shows a comparison of the meridional winds derived from COSMIC observed hmF_2 and NmF_2 (referred to as COSMIC winds) with ISR and FPI technique winds (if available) and also the TIE-GCM. The results are for the four stations: Millstone Hill, Saint Santin, Arecibo, and Shigariki (MU radar). As mentioned before, the ISR and FPI winds are the averaged results of many years under solar minimum, winter conditions. Note that at Arecibo, the COSMIC winds (blue-dashed) are also presented with the effects of north-perpendicular E × B drifts excluded using the observed average pattern under similar geophysical conditions (see detail in the thesis of *Scherliess* [1997], Figure 3.8 in chapter 3). The standard derivation of FPI winds presented here is generally about 30 m/s; and that of the ISR winds is mostly much smaller than 30 m/s over Shigariki [*Kawamura et al.*, 2000], around 30 m/s over Millstone Hill according to the work of *Hagan* [1993], and a litter higher than 30 m/s over Saint Santin [*Duboin and Lafeuille*, 1992].

[16] Over Millstone Hill, the COSMIC winds are compared with the ISR winds, FPI winds (south-looking and north-looking), and also TIE-GCM winds. At night, the COSMIC winds have comparable velocity with TIE-GCM, and this feature is similar at the other three stations. It is noted that the south-looking (∼40°N) and north-looking (∼45°N) FPI winds exhibit a distinct difference in velocity during 2300–0400 LT, which can be as large as 50 m/s. The COSMIC wind velocity is between the south-looking and north-looking FPI winds after midnight. The ISR winds clearly have a larger velocity than the others during 2100–0100 LT. During the daytime, the winds from COSMIC and TIE-GCM are also comparable, and the COSMIC winds are about 1.5 to 2 times larger than the ISR winds but have a similar temporal variation. There is distinctly more equatorward velocity of COSMIC winds than all other winds in the sunset hours near 1800 LT. This feature can be also seen over Saint Santin and Arecibo. As a result, the transition from poleward to equatorward winds occurs earlier for the COSMIC winds. Over Saint Santin, the winds exhibit good agreement between COSMIC, ISR, and TIE-GCM, except during sunset hours. It is noted that a larger Burnside factor (∼1.7) is used to obtain the Saint Santin ISR winds [*Duboin and Lafeuille*, 1992], which corresponds to a higher ion-neutral collision frequency and decreases the wind velocity more than the one used at present study, especially at night.

[17] Comparison of meridional winds at lower midlatitudes is also presented at Shigariki and Arecibo. Over Arecibo, the agreement is generally good. However, the COSMIC winds transit from poleward to equatorward about 1 h earlier than FPI and TIE-GCM winds, and also have larger velocity from the evening to midnight. In addition, the COSMIC winds show some fluctuations during daytime and it is evident that the COSMIC wind velocity is about half of the value of the winds when **E** × **B** drifts are excluded during 1000–1200 LT. At Shigariki, the COSMIC winds are compared with ISR and TIE-GCM winds. The results show general agreement among these winds, but large midnight discrepancies occur between ISR and other winds, and large noon ones occur between COSMIC and other winds. The Shigariki station locates at the similar magnetic latitude to Arecibo, but at midnight the ISR wind velocities over Shigariki are much higher than those of the FPI winds over Arecibo. The COSMIC winds have good agreement with ISR winds during the transition between daytime and nighttime, but exhibit much smaller magnitudes during a few hours around noon. This discrepancy may be caused by complex effects including electric field drifts.

[18] Overall, reasonable agreement between wind estimates from various methods is generally obtained at each station. The COSMIC winds almost match the others in both the diurnal pattern and wind velocity, except for a few discrepancies at particular local times. The COSMIC winds show higher equatorward velocity than those from other techniques near sunset hours at most stations. Also the COSMIC winds tend to have many temporal fluctuations, some of which are similar to the ISR winds. Some of these fluctuations may be induced by electric field drifts since the COSMIC winds are equivalent winds including E × B drifts, as discussed below in section 4.1. The uneven distribution of the observational data may also induce some fluctuations.

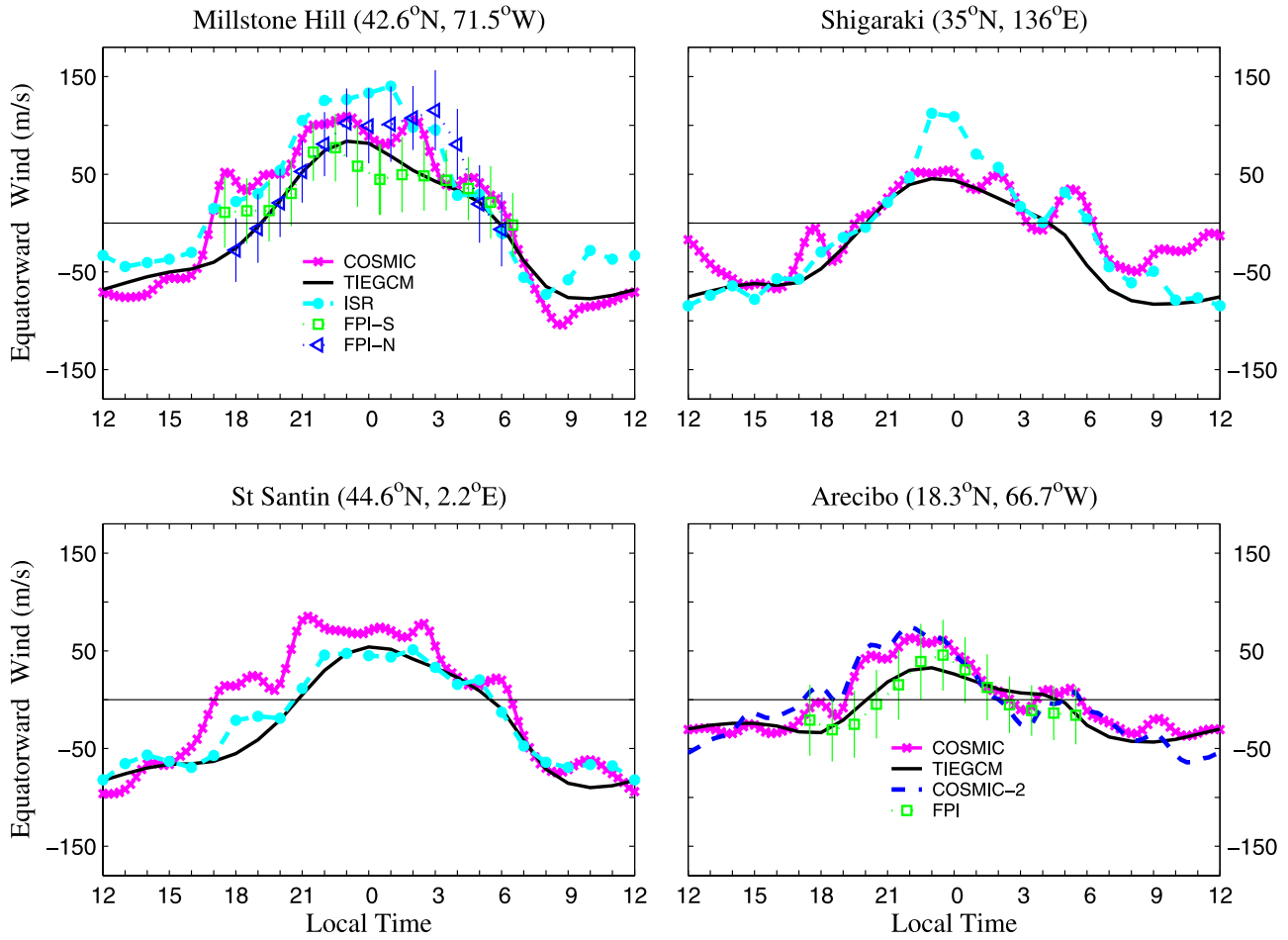

Figure 2. The comparison of the average meridional winds derived from the servo method (COSMIC or COSMIC-2), ISR and/or FPI techniques (FPI, FPI-N or FPI-S, with standard deviations), and the TIE-GCM simulation at the stations of Millstone Hill, Saint Santin, and Shigaraki (MU radar) and Arecibo in winter, solar minimum conditions. The legends for the winds at Saint Santin and MU radar are the same as that at Millstone Hill. The COSMIC-2 (blue dashed) at Arecibo represents COSMIC winds in which the effects of E × B are excluded using the observed average drift pattern under solar minimum winter condition [*Scherliess*, 1997]. The ISR and FPI winds are the average from many years of observations (see detail in the text). The winds are positive equatorward.

3.2. Longitudinal Variation of Meridional Winds

[19] Figure 3 shows longitudinal variations derived from COSMIC observations and simulation results of the TIE-GCM model at 40°N (local winter), including meridional winds and the corresponding F_2 layer peak height as a function of longitude and local time. Both the longitudinal variations of the hmF_2 and winds are significant and local-time dependent. Strong longitudinal variations in COSMIC winds are found around the midnight sector with the wind velocity difference as large as 80 m/s between different longitudes, and during late morning hours before noon with the velocity difference as large as 40 m/s. From late evening to early morning hours (2100–0300 LT), larger winds of 70–110 m/s occur within the longitude range of 110°W–20°W (northern American-Atlantic sector) with a maximum velocity occurring near longitude 60°W. A second maximum around 70 m/s occurs near 2200–0100 LT within the longitude range 100°E to 170° in the Asian-Pacific sector. A general wind speed of 30–50 m/s is present at other longitude sectors near midnight. Large horizontal wind gradients occur from longitude 120°W to 0°. During the daytime, the winds are also larger at longitudes between 130°W and 30°E with a maximum value of −70 m/s (poleward) occurring near 60°W. It is notable that the largest wind speed during the daytime and nighttime peaks near longitude 60°W, where the largest negative magnetic declination angle locates. In section 4.2, it is shown that the longitudinal structure of winds is closely associated with the magnetic declination angle and the influence of zonal wind.

[20] The TIE-GCM winds show similar longitudinal variations during the night, except the wind speed is smaller at all longitudes and the local time duration of maximum wind is shorter near the northern American-Atlantic sector than COSMIC winds. The TIE-GCM winds have a primary peak of 50–70 m/s in the 120°W–20°W longitude range, lasting from 2200 LT to 0200 LT, and a secondary peak of 50 m/s within the 90°E–170°E longitude range. However, there is no evident longitudinal variation for TIE-GCM

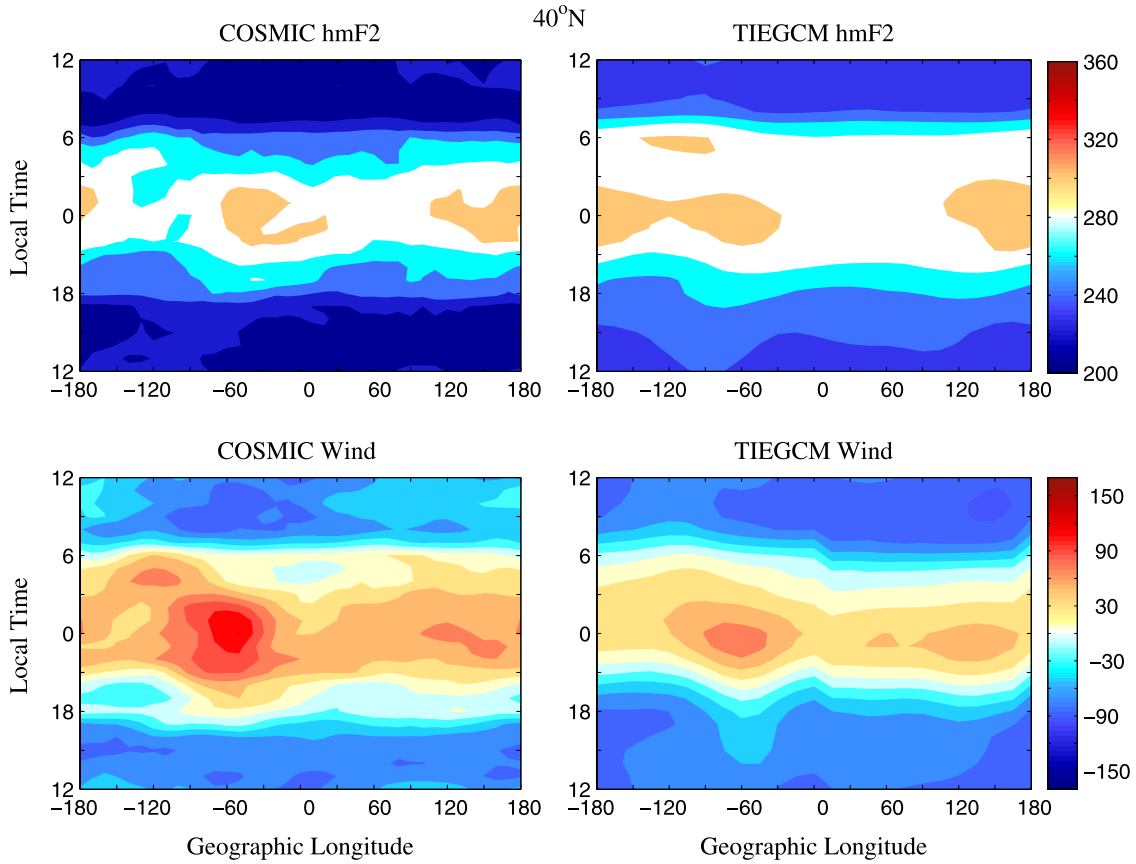

Figure 3. Comparison of longitudinal variations of the F_2 layer peak height, hmF_2 (top, unit: km) and magnetic meridional winds (bottom, unit: m/s) as a function of local time between the COSMIC derived and TIE-GCM model at 40°N in local winter. The contour interval is 20 km for hmF_2 and 20 m/s for winds. The winds are positive equatorward.

winds during the later morning hours, but a minimum wind peak occurs around 60°W during 1400–1900 LT. During the night, similar longitudinal variation of the F_2 layer peak height is seen in both the COSMIC data and the TIE-GCM simulation. During the daytime, there are no obvious longitudinal variations in either the COSMIC or the TIE-GCM hmF_2. The longitudinal sectors of maximum peak height generally shift a little from those of maximum meridional winds.

[21] Figure 4 shows a comparison similar to Figure 3, but for 40°S in local summer. The longitudinal variations in winds and hmF_2 are pronounced during day and night and different from those at 40°N. The COSMIC winds are characterized by much larger poleward winds in the 120°E–110°W sector than in other sectors during the daytime and a local time shift of the nighttime maximum equatorward winds by ~2 h between the 60°W–90°E and 120°E–90°W sectors. At 120°E–110°W sector, the COSMIC winds are poleward with a velocity of 40–60 m/s from sunrise to midafternoon (0600–1500 LT). At the same local time, however, in the other longitudinal sectors (120°W–90°E) the winds are weak with velocities near zero. During the night the maximum equatorward winds occur at different local times between different longitudinal sectors, although the maximum wind velocities are comparable. Therefore at the same local time, the wind velocity difference between different longitudes is estimated to be as large as 80 m/s during the night and 60 m/s during the daytime. The largest longitudinal gradient of winds occurs in the evening sector in the longitudes between 90°E–130°E. The TIE-GCM winds show similar longitudinal variations, except that the winds are generally about 20 m/s larger, and the maximum equatorward winds last longer in local time in most longitudes during nighttime. For the F_2 layer peak height from both the COSMIC data and TIE-GCM simulation, the longitudinal dependence is similar to that of the winds during the daytime, while during night there is a long duration in local time of higher peak heights in most regions of the western hemisphere.

[22] There are some differences between the maximum speed of COSMIC and TIE-GCM winds in temporal duration and also longitudinal span during day and night. However, the greatest discrepancy between COSMIC and TIE-GCM winds is the longitudinal variation in the late morning (0800–1200 LT) and late afternoon (1400–1900 LT) hours at 40°N. The velocity differences between the COSMIC and TIE-GCM winds may be partly induced by differences in electron density and the consequent ion drag [*Lei et al.*, 2007b].

[23] It is noted that the location of the maximum (or minimum) of meridional winds derived from COSMIC observations has a clear shift in longitude from that of

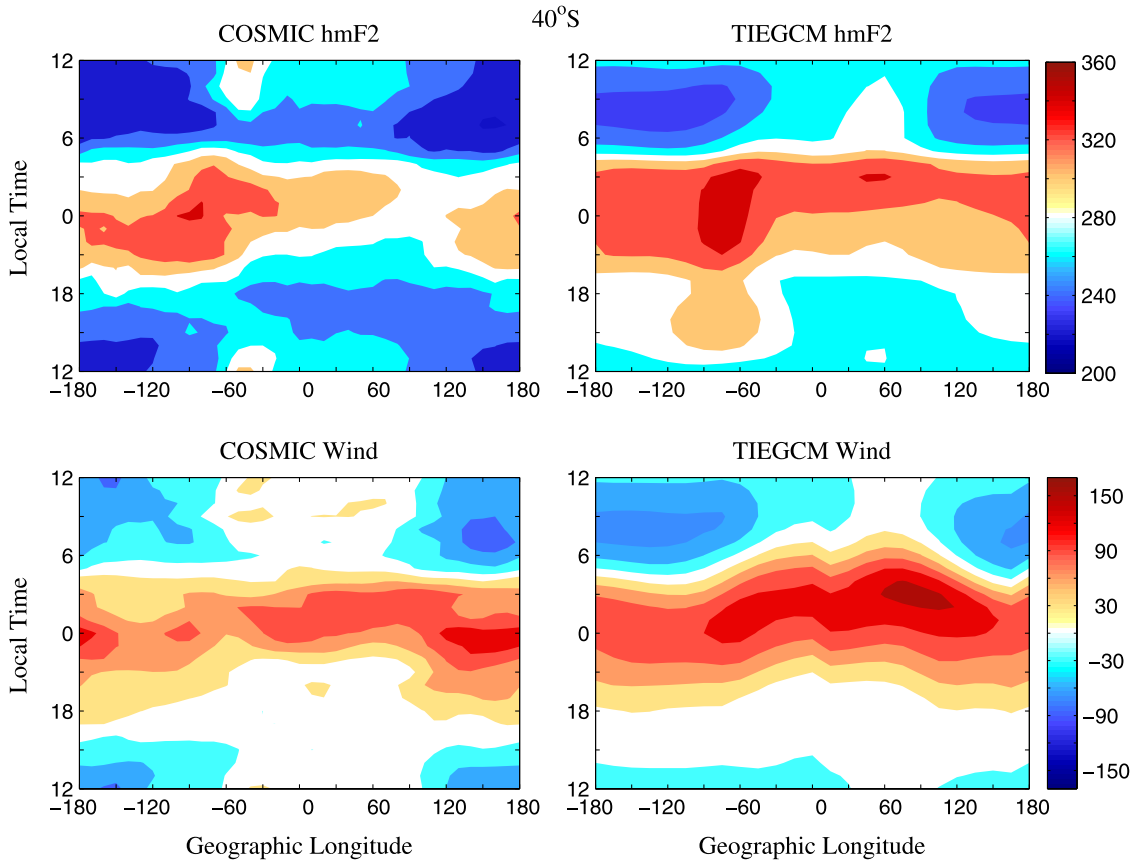

Figure 4. Same as Figure 3, but for 40°S in local summer and the wind contour interval is 30 m/s.

hmF_2, especially in the Southern Hemisphere during night, which is similar to the TIE-GCM results. This may be largely attributed to the differences in magnetic inclination in the different longitude sectors. Recently, *Karpachev and Gasilov* [2006] found that vertical drifts (W) calculated from the servo method have maximum (or minimum) values in the same longitude sectors as those of hmF_2, based on Intercosmos-19 satellite observations.

[24] Figure 5 shows the longitudinal variation of meridional winds from the HWM93 model at 40°N and 40°S under the same solar and geomagnetic activity condition as the COSMIC winds. The HWM93 winds are calculated at the F_2 layer peak height derived from COSMIC observations. The HWM93 winds exhibit a distinct difference of major longitudinal structure from COSMIC and TIE-GCM winds during night. At 40°N, the HWM93 model produces comparable equatorward wind speed near midnight within the longitude range 110°W–160°E; hence the wind speed differences are small from the American sector to the Asian-Pacific sector. At 40°S, HWM93 has large, long duration (~5–10 h) equatorward winds from late evening to noon within the longitude range of 90°W–160°E. However, at 40°N the HWM93 winds show clearly larger poleward winds in the northern American-Atlantic sector before noon than at other longitudes, similar to the COSMIC winds; and the HWM93 winds show minimum wind peak during 1400–1900 LT in the northern American-Atlantic sector, similar to TIE-GCM winds. At 40°S, the longitudinal structure of winds during the daytime is similar to that from COSMIC or TIE-GCM. Also, both the TIE-GCM and the HWM93 winds have nighttime peaks in the longitudinal sector 50°E–90°E at 40°S, which is different from the COSMIC winds.

4. Discussion

4.1. Evaluation of the COSMIC Winds

[25] Generally good agreement has been obtained between the COSMIC and other winds, although there are some limitations in the winds derived from servo methods. This result is similar to the comparison by *Buonsanto et al.* [1997] over Millstone Hill using 34 ISR experiments under both solar minimum and solar maximum conditions. The assumption of steady state of the ionosphere F layer limits the COSMIC winds derived from servo method to magnetically undisturbed conditions. Possible errors of winds from the servo method can be induced by the effect of the $\mathbf{E} \times \mathbf{B}$ drifts and also errors involving the balance height from sunrise to late afternoon hours [*Titheridge*, 1995]. Under some extreme conditions, a low hmF_2 will be incorrectly interpreted as the effect of poleward wind, when the peak in the altitude distribution of O^+ is higher than the F_2 layer peak height [*Buonsanto*, 1990; *Buonsanto et al.*, 1997]. In addition, the wind calculated from the servo method is sensitive to the hmF_2, i.e., 10 km uncertainty of hmF_2 can cause a maximum uncertainty of ~20 m/s of the derived winds [*Titheridge*, 1993]. In average conditions and under magnetic quiet conditions, these limitations seem to have insignificant effects on the derivation of the winds from

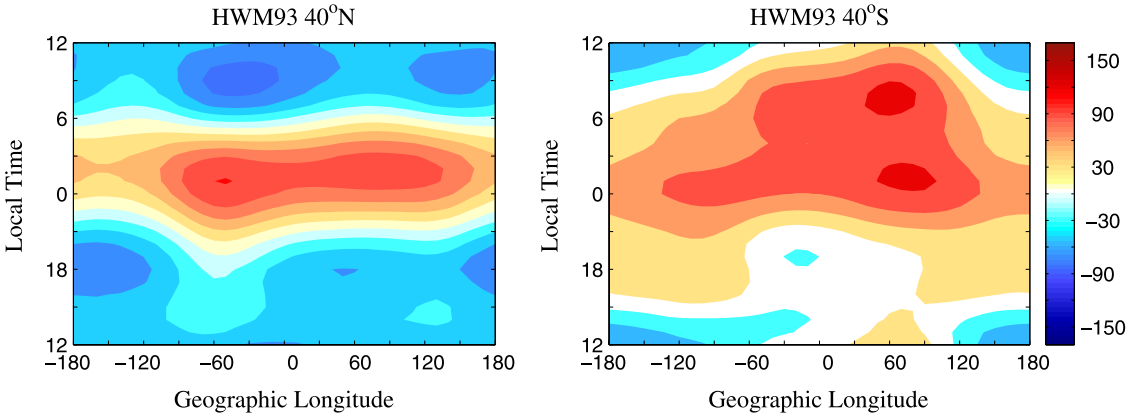

Figure 5. The longitudinal variations of the meridional winds at the F_2 layer peak height predicted by HWM93 model at 40°N (left) and 40°S (right) in winter at solar minimum.

COSMIC observations except for the effect of the **E** × **B** drifts.

[26] The COSMIC winds include the effects of the **E** × **B** drifts by the value of $V_N/\sin I$ in equation (2), which can be the possible source of significant discrepancy between winds, especially at lower latitudes. Long duration upward **E** × **B** drifts with average speeds between 10–25 m/s during 0900–1300 LT have been reported over Shigariki, Japan [*Zhang et al.*, 2001] and Arecibo [*Fejer*, 1993; *Scherliess*, 1997] at solar minimum in winter, while the perpendicular north **E** × **B** drifts are not so significant over Millstone Hill and Saint Santin [*Buonsanto and Witasse*, 1999; *Blanc and Amayenc*, 1979]. Besides, the wind velocity is relatively larger at these two midlatitudes of Millstone Hill and Saint Santin, hence it further limits the relative contribution from the **E** × **B** drifts. At Arecibo, the contribution of **E** × **B** drifts is about 30 m/s during 1000–1200 LT, which is comparable to the equivalent wind velocity (Figure 2). At Shigariki, there is a great velocity discrepancy of more than 50 m/s between COSMIC winds and ISR and TIE-GCM winds at the station of Shigariki around noon (Figure 2). This may be partly explained by the **E** × **B** drifts. In addition, as mentioned before, there is less observational data sampling during a few hours after noon at this station. At Shigariki, *Igi et al.* [1995] compared winds between the ISR technique and those estimated from nearby ionosonde observations during 1986–1988 and found good agreement in all seasons including winter, while *Kawamura et al.* [2000] found cases of great discrepancy at solar maximum in winter between the ISR and equivalent winds derived from ionosonde observations without correction by observational **E** × **B** drifts. Much caution at lower latitudes is needed to analyze the equivalent winds during daytime, when the wind velocity is relatively smaller and the contribution of **E** × **B** drifts is significant.

[27] It is interesting to note that we did not find systematically more poleward winds from COSMIC data than the ISR and TIE-GCM winds in the Northern Hemisphere (Figures 2 and 3), even though the peak height retrieved from COSMIC seems to be 10–20 km lower than the IRI model and TIE-GCM during the daytime at middle latitudes [see Figure 7 of *Lei et al.*, 2007a]. Similar hmF_2 differences between COSMIC and TIE-GCM are seen in Figure 3. In the Southern Hemisphere, however, the COSMIC winds are more poleward than the TIE-GCM winds during afternoon hours (1200–1500 LT), when the hmF_2 from COSMIC is about 20–40 km lower than that simulated from the TIE-GCM.

[28] Although there are a few limitations of the equivalent winds derived from F_2 layer peak parameters, a broader insight on the meridional winds has been achieved by this study. It is noticed that for the winds derived from COSMIC observations, some fluctuations may be induced by the uneven observational sampling, such as the observations during early morning hours over Millstone Hill. In addition, it should be pointed out that the IRI model, which the servo method relies on to provide the ion and electron temperatures in the balance height calculation, has less ground-based data in the Southern Hemisphere, which may have some effect on the wind calculations from COSMIC observations.

4.2. Effect of the Magnetic Declination on the Longitudinal Variations of the Winds

[29] In recent years, several studies have put more or less importance on the magnetic strength or declination angle in the longitudinal characteristics of the vertical ion drifts and ion density in the ionosphere from satellite-based observation [e.g., *de Paula et al.*, 2002; *Vichare and Richmond*, 2005; *Kil et al.*, 2006; *Hartman and Heelis*, 2007]. Here, we investigate the effect of the magnetic declination on the longitudinal variations of the neutral winds. Figures 6 and 7 compare the magnetic meridional winds from TIE-GCM model in different longitude sectors of positive and negative declinations at 40°N and 40°S, respectively. The corresponding geographic North-south winds (equatorward positive) and zonal winds (eastward positive) are also presented. At both 40°N and 40°S, a common feature is that marked differences in the wind velocity occur between longitudes of opposite magnetic declinations.

[30] At 40°N, the nighttime main peak and secondary peak of equatorward winds occur at longitudes with maximum and secondary maximum negative magnetic declinations, respectively. Similarly, at 40°S, the peak of poleward meridional winds during late morning hours can be seen at longitudes with positive declinations. For the nighttime equatorward winds at 40°S, a peak occurs at longitudes

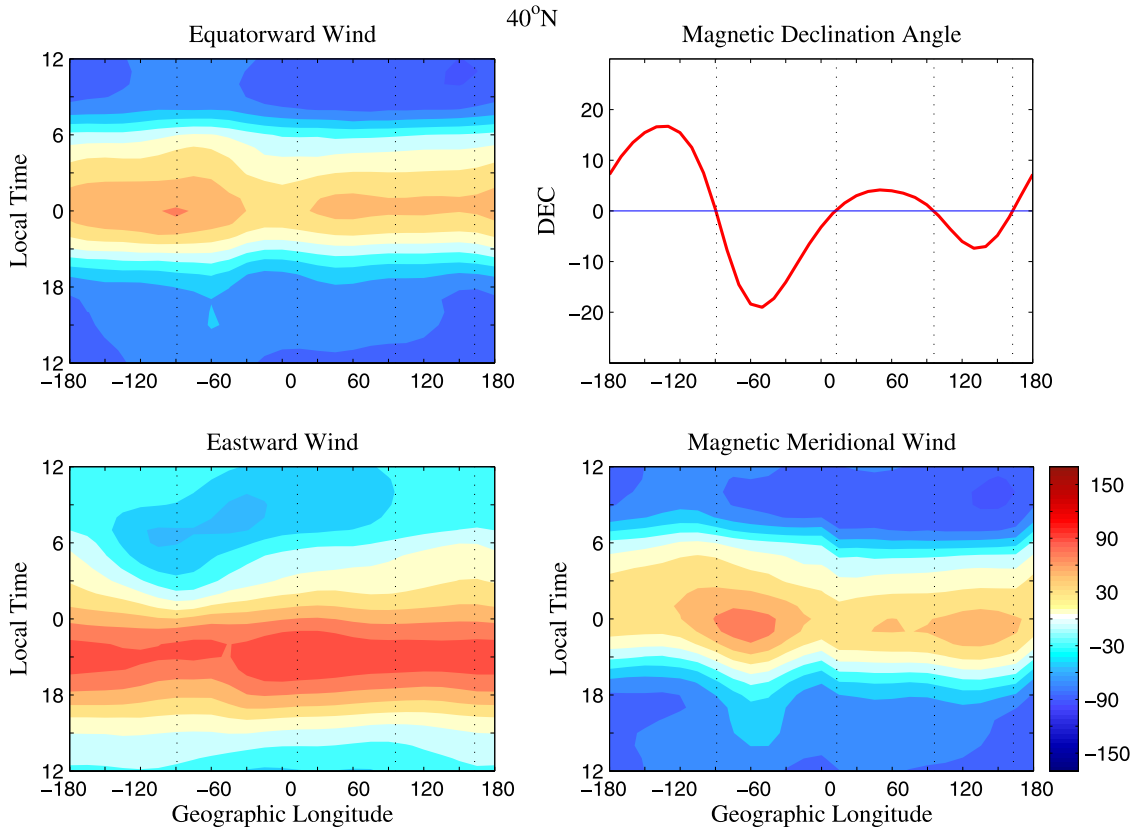

Figure 6. Effect of the magnetic declination (DEC) on the longitudinal variations of the meridional winds from TIE-GCM simulation at 40°N. The Magnetic Meridional wind is the same TIE-GCM wind as Figure 3. The north-south winds (positive equatorward) and zonal winds (positive eastward) are in geographic coordinates. The contour interval is 20 m/s for all winds.

with maximum negative declination and the nighttime maximum velocity shifts about 1–2 h later in the negative declination sector compared to those at longitudes of positive declination. This can be generally explained by the effect of the magnetic declination and also the seasonal pattern of geographic north-south and zonal winds as follows.

[31] At midlatitudes, as shown by Figures 6–7, the north-south (in geographic meridian) winds have a general pattern of equatorward around midnight hours and poleward around noon hours. The zonal winds tend to be eastward before midnight and westward after midnight. The transition time of both winds varies with season. However, around midnight and noon, the directions of the north-south winds are stable, while the zonal winds are seasonally dependent. In the winter hemisphere (40°N) the zonal winds during the night are first strongly eastward and then transit to weakly westward mostly after about 0300 LT, while in the summer hemisphere they change form weakly eastward to strongly westward around midnight. According to equation (3), in comparison with the north-south winds, the magnetic meridional winds can be strengthened in the regions where the contributions from zonal and north-south winds are in the same direction, and vice versa. Figure 8 presents a schematic diagram of the effect of the geomagnetic declination angle on the magnetic meridional winds around midnight hours at 40°N. During midnight period the north-south winds (V_G) are equatorward/southward and the zonal winds (U_G) are eastward. As a result, the zonal winds have a positive contribution to the magnetic meridional winds (U_M) in the longitudes of negative (westward) declination and they have a negative contribution in the longitudes of positive (eastward) declination. It can explain the marked longitudinal variation of the meridional winds in the midnight sector. Similarly, during late morning hours at 40°N, both the north-south winds and zonal winds change to the opposite directions, then the magnetic meridional winds tend to be strengthened in the same regions as during midnight. However, during the late morning hours, there are no significant poleward meridional winds near negative declination sectors for the TIE-GCM results. This feature is different from that of COSMIC winds. In the same way as at 40°N, in the Southern Hemisphere the zonal winds tend to have a positive contribution at the positive declination (eastward) sector in the late morning hours, in condition of geographic poleward/southward winds and westward winds, building large morning poleward meridional winds. Also, the strong, earlier westward zonal winds have a positive contribution to the equatorward/northward meridional winds during early morning hours near the negative declination sector, resulting in the local time shift of the nighttime maximum equatorward winds.

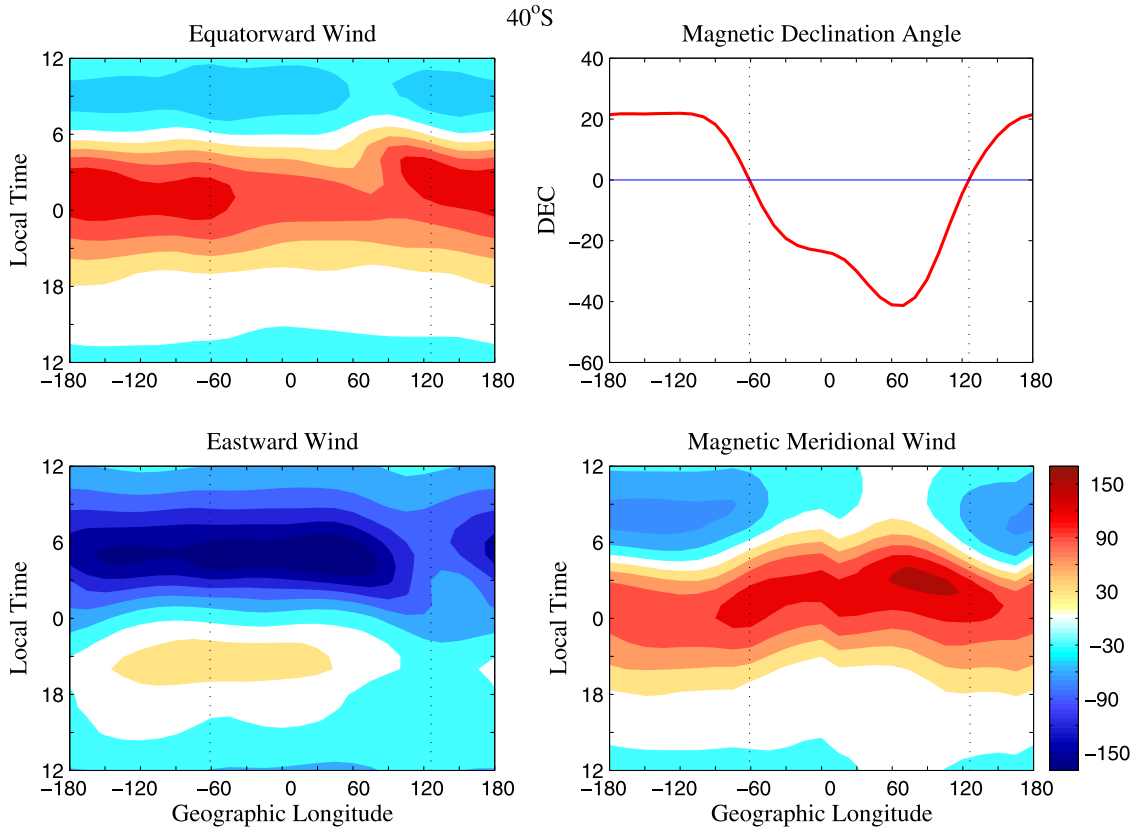

Figure 7. Same as Figure 6, but for 40°S.

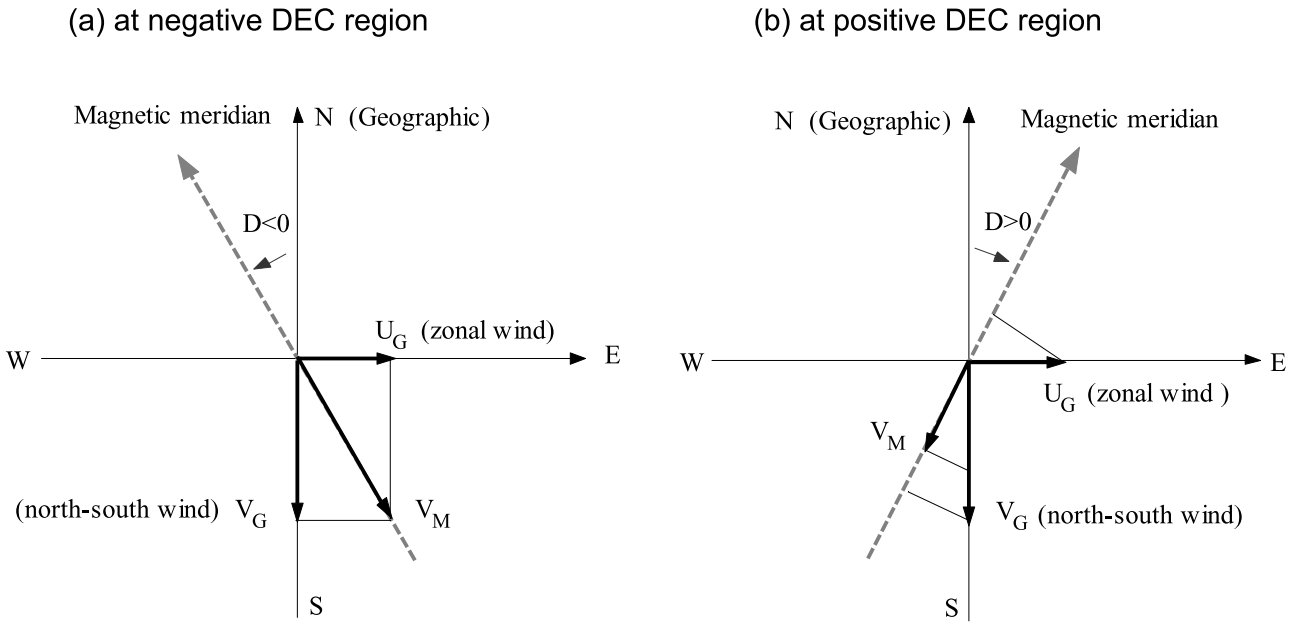

Figure 8. A schematic diagram of the effect of the geomagnetic declination angle (DEC, and "D" in the diagram) on the magnetic meridional winds around midnight hours at 40°N. (a) for negative DEC region and (b) for positive DEC region. N, S, E, and W represent northward, southward, eastward, and westward directions in the geographic coordinate, respectively. V_M, U_G and V_G represent magnetic meridional wind, zonal wind and north-south wind, respectively.

[32] The longitudinal variation of neutral winds is practically unexplored and its mechanism is far from clear. *Wu et al.* [1994] found no clear relationship between the longitudinal variations of the neutral temperature and the zonal winds from DE-2 observations. From the TIE-GCM results, the longitudinal variations of the north-south and zonal winds are not very significant at the northern winter hemisphere, while they do show some features in the southern summer hemisphere. This phenomenon may be related to the longitudinal variations of the electron density, because the subsequent ion drags at different longitudes are expected to have some effects [*Liu et al.*, 2004]. According to equation (3), the longitudinal variation of the meridional winds in the magnetic meridian can be expected even in the absence of any longitudinal variation of winds in geographic coordinate. Consequently, the longitudinal variations of magnetic meridional winds can lead to longitudinal variations of the electron density and other upper thermosphere/ionosphere parameters, which in turn can complicate the longitudinal variations of neutral winds. It is evident that, due to the modulation of the magnetic declination, the longitudinal variations of the magnetic meridional winds are much more distinct and significantly different in comparison with the north-south winds (Figures 6–7). In addition, some of the longitudes are in higher magnetic latitudes nearer to the magnetic poles, where the winds may be also affected by the high latitude convection, as suggested by *Emmert et al.* [2003].

[33] The TIE-GCM results suggest that the longitudinal variations of meridional winds are mostly contributed to by the large geographic zonal winds at certain preferred longitudinal sectors with either positive or negative magnetic declination. Similar to the TIE-GCM winds, most of the longitudinal variations of the COSMIC winds can also be explained by the effect of the magnetic declination on the basis of the day to night pattern of the neutral winds in each season, except for no stronger nighttime wind peak around 60°E sectors than other longitudes at 40°S. The 60°E sector at 40°S is where the maximum negative declination locates and nighttime wind peak was predicted by TIE-GCM and HWM93 model.

[34] Besides the seasonal variation of neutral winds, the different longitudinal patterns of magnetic meridional winds between Northern and Southern Hemisphere are also caused by difference in magnetic field and in geographic direction of the equatorward or poleward winds. Note that at 40°S the longitudes of positive and negative declination angle are different from those at 40°N and the declination angles are much larger (Figures 6 and 7). Also the nighttime equatorward winds are in the northward direction at 40°S, while they are in the southward direction at 40°N. This difference is similar during daytime. Hence even for the same direction of zonal wind and same sign of declination, the contribution of the zonal wind to the magnetic meridional wind is opposite between the Northern and Southern Hemisphere. The meridional winds are most likely to occur strongly at regions of large declination and in seasons with large zonal wind, indicating complex seasonal and hemispheric dependences for their longitudinal patterns. Longitudinal variations of the neutral winds need more investigations. Using the global COSMIC observations, further study can be carried out on the longitudinal variation of the magnetic meridional winds for different latitudes and seasons at both hemispheres.

5. Summary and Conclusion

[35] The F_2 layer peak height (hmF_2) and peak density (NmF_2) retrieved from the COSMIC radio occultation measurements are used to derive the magnetic meridional winds (COSMIC winds). The average winds in four winter months in the solar minimum years of 2006–2007 are compared with those derived from other observational data at four stations (Millstone Hill, Saint Santin, Arecibo, and Shigariki) and the TIE-GCM. The longitudinal variations of the derived winds are analyzed at the midlatitudes of 40°N in local winter and 40°S in local summer. The summary and conclusion include:

[36] 1. Good agreement between the COSMIC winds and those from ISR, FPI measurements, and TIE-GCM simulations is generally obtained at the selected stations. However, great discrepancy in wind velocity occurs around noon hours at Shigaraki and Arecibo.

[37] 2. Significant longitudinal variations seen in the COSMIC winds at both 40°N (local winter) and 40°S (local summer) are mostly reproduced by the TIE-GCM. Compared with winds predicted by the HWM93, these variations are similar during daytime but inconsistent during night.

[38] 3. At 40°N, the COSMIC winds have large velocities around the midnight hours and during late morning hours within the longitude range of negative magnetic declination (110°W–20°W), which corresponds to the North American-Atlantic sector. A second but weak peak velocity also occurs at night within the longitude range of negative magnetic declination (110°E –170°E), which corresponds to the Asian sector.

[39] 4. At 40°S, the COSMIC winds are poleward and characterized by large velocities from sunrise to afternoon hours within the positive declination sector (120°E–110°W). At night, the peak equatorward winds shift about 2 h later in local time in the longitudes within the negative declination sectors (60°W–90°E) compared to winds at other longitudes within positive declination.

[40] 5. TIE-GCM simulations of the neutral winds in both the magnetic and geographic coordinates reveal that most of the longitudinal variations of the magnetic meridional winds are due to the effects of zonal wind and the magnetic declination.

[41] **Acknowledgments.** The authors thank Drs. Jiuhou Lei, Wenbin Wang, and Barbara Emery for helpful discussions, and Xiaoli Luan also thanks Dr. Libo Liu for drawing her attention to this topic. Development of the COSMIC Data Analysis and Archival Center (CDAAC) is primarily supported by the National Science Foundation and the National Oceanic and Atmospheric Administration. COSMIC data are provided by Taiwan's National Space Organization (NSPO) and the University Corporation for Atmospheric Research (UCAR). The used ISR wind data at Millstone Hill, Saint Santin and MU Radar were provided by Dr. Seji Kawamura. The FPI data were obtained from the CEDAR Database at the National Center for Atmospheric Research, which is supported by the National Science Foundation. This research was also supported by NASA grant NNX07AC55G to the University Corporation for Atmospheric Research.

[42] Wolfgang Baumjohann thanks the reviewers for their assistance in evaluating this paper.

References

Banks, P. (1966), Collision frequencies and energy transfer: Ions, *Planet. Space Sci.*, *14*, 1105–1122.

Bilitza, D. (2001), International reference ionosphere 2000, *Radio Sci.*, *36*(2), 261–275.

Biondi, M. A., S. Y. Sazykin, B. G. Fejer, J. W. Meriwether, and C. G. Fesen (1999), Equatorial and low latitude thermospheric winds: Measured quiet time variation with season and solar flux from 1980 to 1990, *J. Geophys. Res.*, *104*(A8), 17,091–17,106.

Blanc, M., and P. Amayenc (1979), Seasonal variations of the ionospheric $\mathbf{E} \times \mathbf{B}$ drifts above Saint Santin on quiet days, *J. Geophys. Res.*, *84*(A6), 2691–2704.

Buonsanto, M. J. (1990), Observed and calculated F_2 peak heights and derived meridional winds at mid-latitudes over a full solar cycle, *J. Atmos. Sol. Terr. Phys.*, *52*, 223–240.

Buonsanto, M. J. (1991), Neutral winds in the thermosphere at mid-latitude over a full solar cycle: A tidal decomposition, *J. Geophys. Res.*, *96*(A3), 3711–3724.

Buonsanto, M. J., and O. G. Witasse (1999), An updated climatology of thermospheric neutral winds and F region ion drifts above Millstone Hill, *J. Geophys. Res.*, *104*(A11), 24,675–24,687.

Buonsanto, M. J., J. E. Salah, K. L. Miller, W. L. Oliver, R. G. Burnside, and P. G. Richards (1989), Observations of neutral circulation at mid-latitudes during the equinox transition study, *J. Geophys. Res.*, *94*(A12), 16,987–16,997.

Buonsanto, M. J., M. J. Starks, P. G. Richards, and K. L. Miller (1997), Comparison of techniques for derivation of neutral meridional winds from ionospheric data, *J. Geophys. Res.*, *102*(A7), 14,477–14,484.

Burnside, R. G., C. A. Tepley, and V. B. Wickwar (1987), The O+–O collision cross-section: Can it be inferred from aeronomical measurements?, *Ann. Geophys.*, *5*, 343–350.

Deminova, G. F. (2002), Asymmetry of the longitudinal effect in the low-latitude ionosphere, *Adv. Space Res.*, *29*, 911–915.

de Paula, E. R., J. R. Souza, B. G. Fejer, G. J. Bailey, and R. A. Heelis (2002), Longitudinal ionospheric effects in the South Atlantic evening sector during solar maximum, *J. Geophys. Res.*, *107*(A7), 1102, doi:10.1029/2001JA000298.

Duboin, M. L., and M. Lafeuille (1992), Thermospheric dynamics above Saint-Santin: Statistical study of the data set, *J. Geophys. Res.*, *97*(A6), 8661–8671.

Emmert, J. E., B. G. Fejer, and D. P. Sipler (2003), Climatology and latitudinal gradients of quiet time thermospheric neutral winds over Millstone Hill from Fabry-Petrot interferometer measurements, *J. Geophys. Res.*, *108*(A5), 1196, doi:10.1029/2002JA009765.

Emmert, J. T., M. L. Faivre, G. Hernandez, M. J. Jarvis, J. W. Meriwether, R. J. Niciejewski, D. P. Sipler, and C. A. Tepley (2006), Climatologies of nighttime upper thermospheric winds measured by ground-based Fabry-Perot interferometers during geomagnetically quiet conditions: 1. Local time, latitudinal, seasonal, and solar cycle dependence, *J. Geophys. Res.*, *111*, A12302, doi:10.1029/2006JA011948.

Fejer, B. G. (1993), F region plasma drifts over Arecibo: Solar cycle, seasonal, and magnetic activity effects, *J. Geophys. Res.*, *98*(A8), 13,645–13,652.

Foppiano, A. J., X. A. Torres, M. A. Arriagada, and P. A. Flores (2003), Meridional thermospheric winds over the Antarctic Peninsula longitude sector, *J. Atmos. Sol. Terr. Phys.*, *65*, 305–314.

Forbes, J. M., D. Revelle, X. Zhang, and R. E. Markin (1997), Longitude structure of the ionosphere *F* region from TOPEX/Poseidon and ground-based data during January 20–30, 1993, including the quasi 2-day oscillation, *J. Geophys. Res.*, *102*(A4), 7293–7300.

Hagan, M. E. (1993), Quiet time upper thermospheric winds over Millstone Hill between 1984 and 1990, *J. Geophys. Res.*, *98*(A3), 3731–3739.

Hartman, W. A., and R. A. Heelis (2007), Longitudinal variations in the equatorial vertical drift in the topside ionosphere, *J. Geophys. Res.*, *112*, A03305, doi:10.1029/2006JA011773.

Häusler, K., H. Lühr, S. Rentz, and W. Köhler (2007), A statistical analysis of longitudinal dependences of upper thermospheric zonal winds at dip equator latitudes derived from CHAMP, *J. Atmos. Sol. Terr. Phys.*, *69*, 1419–1430.

Hedin, A. E., et al. (1991), Revised global model of thermosphere winds using satellite and ground-based observations, *J. Geophys. Res.*, *96*(A5), 7657–7688.

Hedin, A. E., M. J. Buonsanto, M. Codrescu, M.-L. Duboin, C. G. Fesen, M. E. Hagan, K. L. Miller, and D. P. Sipler (1994), Solar activity variations in midlatitude thermospheric meridional winds, *J. Geophys. Res.*, *99*(A9), 17,601–17,608.

Hedin, A. E., et al. (1996), Empirical wind model for the upper, middle and lower atmosphere, *J. Atmos. Sol. Terr. Phys.*, *58*, 1421–1447.

Igi, S., T. Ogawa, W. L. Oliver, and S. Fukao (1995), Thermospheric winds over Japan: Comparison of ionosonde and radar measurements, *J. Geophys. Res.*, *100*(A11), 21,323–21,326.

Igi, S., W. L. Oliver, and T. Ogawa (1999), Solar cycle variations of the thermospheric meridional wind over Japan derived from measurements of hmF2, *J. Geophys. Res.*, *104*(A10), 22,427–22,431.

Karpachev, A. T., and N. A. Gasilov (2006), Causes of longitude-latitudinal variations in the ionospheric F_2-layer maximum in summer nighttime conditions, *Int. J. Geomagn. Aeron.*, *6*, GI2006, doi:10.1029/2005GI000112.

Kawamura, S., Y. Otsuka, S.-R. Zhang, S. Fukao, and W. L. Oliver (2000), A climatology of middle and upper atmosphere radar observations of thermospheric winds, *J. Geophys. Res.*, *105*(A6), 12,777–12,788.

Kil, H., R. De Majistre, L. J. Paxton, and Y. Zhang (2006), Nighttime - region morphology in the low and middle latitudes seen from DMSP F15 and TIMED/GUVI, *J. Atmos. Sol. Terr. Phys.*, *68*, 1672–1681.

Lei, J., et al. (2007a), Comparison of COSMIC ionospheric measurements with ground-based observations and model predictions: Preliminary results, *J. Geophys. Res.*, *112*, A07308, doi:10.1029/2006JA012240.

Lei, J., R. G. Roble, S. Kawamura, and S. Fukao (2007b), A simulation study of thermospheric neutral winds over the MU radar, *J. Geophys. Res.*, *112*, A04303, doi:10.1029/2006JA012038.

Liu, L., X. Luan, W. Wan, B. Ning, and J. Lei (2003a), A new approach to the derivation of dynamic information from ionosonde measurements, *Ann. Geophys.*, *21*(11), 2185–2191.

Liu, L., X. Luan, W. Wan, J. Lei, and B. Ning (2003b), Seasonal behavior of equivalent winds over Wuhan derived from ionospheric data in 2000–2001, *Adv. Space Res.*, *32*, 1765–1770.

Liu, L., X. Luan, W. Wan, J. Lei, and B. Ning (2004), Solar activity variations of equivalent winds derived from global ionosonde data, *J. Geophys. Res.*, *109*, A12305, doi:10.1029/2004JA010574.

Luan, X., L. Liu, W. Wan, J. Lei, and T. Yu (2004), Climatology of the F-layer equivalent winds derived from ionosonde measurements over two decades along the 120°–150°E sector, *Ann. Geophys.*, *22*, 2785–2796.

Miller, K. L., D. G. Torr, and P. G. Richards (1986), Meridional winds in the thermosphere derived from measurement of F_2 layer height, *J. Geophys. Res.*, *91*(A4), 4531–4535.

Miller, K. L., M. Lemon, and P. G. Richards (1997), A meridional wind climatology from a fast model for the derivation of meridional winds from the height of the ionospheric F_2 region, *J. Atmos. Sol. Terr. Phys.*, *59*, 1805–1822.

Picone, J. M., A. E. Hedin, D. P. Drob, and A. C. Aikin (2002), NRLMSISE-00 empirical model of the atmosphere: Statistical comparisons and scientific issues, *J. Geophys. Res.*, *107*(A12), 1468, doi:10.1029/2002JA009430.

Richards, P. G. (1991), An improved algorithm for determining neutral winds from the height of the F_2 peak electron density, *J. Geophys. Res.*, *96*(A10), 17,839–17,846.

Richmond, A. D., E. C. Ridley, and R. G. Roble (1992), A thermosphere/ionosphere general circulation model with coupled electrodynamics, *Geophys. Res. Lett.*, *19*(6), 601–604.

Rishbeth, H. (1967), The effect of winds on the ionospheric F_2-peak, *J. Atmos. Sol. Terr. Phys.*, *29*, 225–238.

Rishbeth, H., S. Ganguly, and J. C. G. Walker (1978), Field-aligned and field-perpendicular velocities in the ionospheric F_2 layer, *J. Atmos. Sol. Terr. Phys.*, *40*, 767–784.

Roble, R. G., E. C. Ridley, A. D. Richmond, and R. E. Dickinson (1988), A coupled thermosphere/ionosphere general circulation model, *Geophys. Res. Lett.*, *15*(12), 1325–1328.

Scherliess, L. (1997), Empirical studies of ionospheric electric fields, Ph.D. thesis, Utah State Univ., Logan, Utah.

Schreiner, W., C. Rocken, S. Sokolovskiy, S. Syndergaard, and D. Hunt (2007), Estimates of the precision of GPS radio occultations from the COSMIC/FORMOSAT-3 mission, *Geophys. Res. Lett.*, *34*, L04808, doi:10.1029/2006GL027557.

Titheridge, J. E. (1993), Atmospheric winds calculated from diurnal changes in the mid-latitude ionosphere, *J. Atmos. Sol. Terr. Phys.*, *55*, 1637–1659.

Titheridge, T. E. (1995), The calculation of neutral winds from ionospheric data, *J. Atmos. Sol. Terr. Phys.*, *57*, 1015–1036.

Vichare, G., and A. D. Richmond (2005), Simulation study of the longitudinal variation of evening vertical ionospheric drifts at the magnetic equator during equinox, *J. Geophys. Res.*, *110*, A05304, doi:10.1029/2004JA010720.

Wu, Q., T. L. Killeen, and N. W. Spencer (1994), Dynamics Explorer 2 observations of equatorial thermospheric winds and temperatures: Local time and longitudinal dependences, *J. Geophys. Res.*, *99*(A4), 6277–6288.

Zhang, S.-R., W. L. Oliver, and S. Fukao (2001), MU radar ion drift model, *Adv. Space Res.*, *27*, 115–120.

X. Luan and S. C. Solomon, High Altitude Observatory, National Center for Atmospheric Research, 3080 Center Green, Boulder, CO 80301, USA. (luanxl@ucar.edu)